Fermi National Accelerator Laboratory

FN-553
[E-687]

Description of Fermilab Experiment E-687 *

The E-687 Collaboration

presented by

S. Gourlay
Fermi National Accelerator Laboratory
P.O. Box 500
Batavia, Illinois 60510

October 1990

* Presented at the XXVth International Conference on High Energy Physics, Kent Ridge, Singapore, August 2-8, 1990.

Operated by Universities Research Association Inc. under contract with the United States Department of Energy

Description of Fermilab Experiment E-687

P.L. Frabetti
Dip. di Fisica dell'Universita' and INFN - Bologna, I-40126 Bologna, Italy

C.W. Bogart, H. Cheung, P. Coteus,[a] S. Culy, J.P. Cumalat, D. Kaplan,[b]
University of Colorado, Boulder, CO 80309, USA

J. Butler, F. Davenport,[c] I. Gaines P. Garbincius, S. Gourlay
D. Harding, P. Kasper, A. Kreymer, P. Lebrun, H. Mendez,
Fermilab, Batavia, IL 60510, USA

S. Bianco, F.L. Fabbri, A. Spallone, A. Zallo,
Laboratori Nazionali di Frascati, I-00044 Frascati, Italy

R. Culbertson, M. Diesburg,[d] G. Jaross, K. Lingel, P. Sheldon, J.R. Wilson,
University of Illinois at Urbana-Champaign, Urbana, IL 61801, USA

G. Alimonti, G. Bellini, M. Di Corato, M. Giammarchi, P. Inzani,
S. Malvezzi, P.F. Manfredi,[e] D. Menasce, E. Meroni, L. Moroni,
D. Pedrini, L. Perasso, F. Ragusa, A. Sala, S. Sala, D. Torretta, M. Vittone[d]
Dip. di Fisica dell'Universita' and INFN - Milano, I-20133 Milan, Italy

D. Buchholz, C. Castoldi,[f] B. Gobbi, S. Park, R. Yoshida
Northwestern University, Evanston, IL 60208, USA

J.M. Bishop, J.K. Busenitz,[g] N.M. Cason, J.D.Cunningham, R.W. Gardner
C.J. Kennedy, E.J. Mannel, R.J. Mountain, D.L. Puseljic,
R.C. Ruchti, W.D. Shephard, M.E. Zanabria
University of Notre Dame, Notre Dame, IN 46556, USA

G.L. Boca, R. Diaferia, S.P. Ratti, P. Vitulo
Dip. di Fisica dell'Universita' and INFN - Pavia, I-27100 Pavia, Italy

A. Lopez
University of Puerto Rico at Mayaguez, Puerto Rico

Presented by S. Gourlay for the Fermilab E687 Collaboration

Description of Fermilab Experiment E-687

Abstract

Fermilab experiment E-687 is a high statistics charm photoproduction experiment in the Wide-Band Photon Laboratory. This paper describes the apparatus used in a recent run from which approximately 10^4 charm decays were reconstructed.

1.0 Introduction

Fermilab experiment 687 utilizes the world's highest energy photon beam and a highly efficient, large acceptance, high rate multiparticle spectrometer to study the production and decay of charmed particles. The two magnet spectrometer features charged particle tracking via silicon microstrip detectors and a proportional wire chamber system. Neutral vees are reconstructed over a 10m decay path. Charged particle identification is accomplished with three multi-celled Cerenkov counters. The system includes detectors to identify photons, electrons and muons over a large range in acceptance. This combination of detectors allows observation of a wide variety of charmed baryon and meson decay modes. In a 5 month run completed in March of 1988, 45 million photon induced hadronic interactions were written on tape. The current data sample is expected to yield approximately 10^4 fully reconstructed charm particles. Examples of some preliminary signals are shown in Figure 1. A description of the E-687 apparatus and performance is given below.

2.0 Beam

2.1 Beamline

The Fermilab wide band beamline (Figure 2) produces a high energy bremstrahlung photon beam with very low hadronic background and a broad energy spectrum (13%) [1,2]. Photons from π^0 decay were produced by 800 GeV protons on an 18" Be target. The photons were passed through a 60% radiation length converter and the resulting electron beam was steered around a neutral particle dump. The electrons then traversed a 27% lead radiator and were swept by a series of dipole magnets into a recoil shower hodoscope (RESH), while the resulting bremstrahlung photons continued to the experimental target. The primary purpose of the RESH was to identify and measure the energy of the incident photon for each event. The tagging resolution was dominated by the 50 GeV spread in the electron energy spectrum. Information from the RESH was also used as part of the second level trigger to impose a minimum requirement on the photon energy spectrum. With the RESH requirement the photon beam

energy had a lower limit of 150 GeV and a mean of 220 GeV (Figure 3). The non-interacting photons were recorded by the Beam Gamma Monitor (BGM), a beam dump calorimeter at the downstream end of the spectrometer used primarily for beam flux and energy monitoring.

2.2 Yields, Backgrounds

The experiment was nominally run with 3 X 10^{12} protons incident on the Beryllium production target yielding approximately 9 X 10^{7} electrons over the 22 second spill of the Tevatron.

Hadronic background is produced via a series of low probability events. The neutral hadron background (the only background of consequence) has been measured and calculated to be 10^{-5} neutrons per photon. Neutron induced hadronic events are therefore less than 1% of the photoproduced hadronic events.

3.0 Spectrometer

The E687 spectrometer (Figure 4) is a general purpose magnetic spectrometer featuring a high resolution silicon vertex detector, Cerenkov particle identification, muon tagging, hadronic and electromagnetic calorimetry.

3.1 Target

The experimental target consisted of Beryllium stacked in 5 blocks each of 8 mm thickness separated by air gaps to give a total length of 4.5 cm and a radiation length of 11.5% (Figure 5).

3.2 Tracking

3.2.1 Microstrips

The charm cross section is about 1% of the total hadronic photon cross section. Coupled with high mean multiplicity this implies that the charm signal sits on a large background. The first real success in the observation of charm at fixed target experiments came with the advent of high resolution Silicon microstrip detectors (SSD's) which make use of the separated charm decay vertex as a means of separating charm events from background. E-687 uses a system (Figure 6) composed of four stations of three planes each, one plane with strips parallel to the spectrometer y-axis and the other two with strips at ±45 degrees. The pitch of the planes in the first station was 25 microns in the central 1/3 of the plane and 50 microns in the outer 2/3, while in the remaining planes the pitch was 50 microns in the central region and 100 microns in the outer. The total system contained approximately 8,000 channels.

The strip signals were read out by front-end amplifiers, remote-end amplifiers and a charge integrating FLASH ADC. The analog readout was

chosen to maximize information for dealing with adjacent hits. Doubling the pitch in the outer regions reduced the number of channels by a factor of two but the track resolution was affected only slightly since the majority of the tracks passed through the high resolution region. The efficiency of each plane was measured to be better than 99% including broken strips and dead channels.

The resolution is expressed as the transverse error extrapolated to the mean interaction point in the target 7 cm upstream of the first microstrip plane. For infinite momentum tracks traversing the high resolution region of the twelve detector planes the resolution is approximately 9 microns. However, in addition to the purely geometric resolution there is a momentum dependent term due to Multiple Coulomb Scattering (MCS). The majority of the scattering was due to the silicon of the microstrip detector with small contributions from the Be target and a trigger counter (TR1).

The overall position resolution is then given by:

$$\sigma_x = 11\mu m \sqrt{1 + \left(\frac{25\ GeV}{p}\right)^2} \qquad \sigma_y = 7.7\mu m \sqrt{1 + \left(\frac{25\ GeV}{p}\right)^2}$$

3.2.2 Multiwire Proportional Chambers

E-687 had 5 multiwire proportional chamber (MWPC) stations for downstream tracking and momentum measurements. They are labeled P0, P1, P2, P3 and P4, upstream to downstream (Figure 4). Each station contained 4 planes (X, Y, U, V). The stereo angle for the U and V views was ±11.3 degrees with respect to the Y view. There were two types of MWPC stations, Type I (P0 and P3) and Type II (P1,P2,P4). The Type I stations had an aperture of 30" x 50" (larger dimension vertical) with 2mm wire spacing. The Type II stations were 60" x 90" with 3mm wire spacing. The P4 chamber was replaced with a smaller chamber (40" x 60") of only three views, X, V and U due to a fire at the beginning of the run. The X plane had 3 mm wire spacing and the U and V views had 2mm wire spacing. The gas was a mixture of 65/35 Argon-Ethane bubbled through ethyl alcohol at 0 degrees C. The preamplified signals for each wire (approximately 13,000) were read out by a LeCroy 4290 TDC system and transferred into a LeCroy 1892 buffer memory via a Fermilab designed interface.

3.2.3 Magnets

Momentum determination of tracks was done using two vertical bending dipole magnets (M1 and M2). The two dipoles were identical except for details of the magnetic shield plates. The first magnet, M1, was operated at a Pt kick of 0.400 GeV/c, and the second magnet (M2), had a Pt kick of 0.850 GeV/c. The two magnets bent in opposite directions with the ratio of

the kicks arranged such that charged tracks return to their original undeflected position in the vicinity of the inner electromagnetic calorimeter.

Resolution for tracks traversing the entire spectrometer is given by:

$$\frac{\sigma p}{p} = 1.4\% \left(\frac{p}{100\ GeV} \right) \sqrt{1 + \left(\frac{23\ GeV}{p} \right)^2}$$

where the $1/p^2$ term is due to MCS and the resolution for tracks passing through M1 only is given by:

$$\frac{\sigma p}{p} = 3.4\% \left(\frac{p}{100\ GeV} \right) \sqrt{1 + \left(\frac{17\ GeV}{p} \right)^2}$$

3.3 Particle ID

3.3.1 Cerenkov

The Cerenkov particle identification system consisted of 3 atmospheric gas filled threshold Cerenkov counters (C1-C3 in Figure 4). Characteristics of the three counters are given in Table 1. The gases have been chosen so that there is a wide range of momentum values in which pions, kaons and protons can be identified. This is critical because identification of kaons and/or protons is crucial for the observation of many of the charm signals present in the data.

Table 1

E-687 Cerenkov counter characteristics

Counter	Gas	Threshold (GeV/c)			No. of Cells
		Pion	Kaon	Proton	
C1	HeN_2	6.7	23.3	44.3	90
C2	N_2O	4.4	16.2	30.9	110
C3	He	17.0	61.0	116.2	100

3.3.2 Muons

The muon detector system (Figures 4,7) is comprised of two sections: An "Inner" section for muons incident at less than 40 mR and an "Outer" section for angles up to 125 mR. The Inner muon (IM) detector consists of two slabs of iron absorber with three scintillator hodoscope planes for triggering, and 4 proportional tube planes for tracking. The iron of the second analysis magnet (M2) serves as the absorber for the Outer muon

system (OM) which includes two scintillator hodoscope planes and two proportional tube planes. The fast muon trigger which was included as part of the second level trigger set was provided by the scintillation counters mounted behind M2 (OMV and OMH) and those mounted behind the muon filter steel downstream of the Hadron Calorimeter (IM1V, IM1H and IM2V) (Figure 4). The data derived from triggers based on the Inner muon system was used for the J/Psi -> 2 muon analysis. The efficiency for reconstructing a single muon was over 95% for events within the geometric acceptance of the muon detectors.

3.3.3 Electromagnetic Calorimetry

The E-687 spectrometer featured large acceptance electromagnetic calorimetry consisting of Inner (IE) and Outer (OE) detectors (Figure 4). The OE provided coverage outside the aperture of the 2nd analysis magnet (M2), while the IE, located downstream of the last chamber station, covered the remaining inner portion.

3.3.4 Hadronic Calorimetry

The primary role of the Hadron Calorimeter (HC) is to provide an additional means of rejecting electromagnetic events and to enhance the fraction of recorded events containing charm.

The calorimeter is constructed of 28 iron plates 120" x 82" x 1.75", separated by a 1.125" gap, totaling 8 proton interaction lengths. Gas sampling sense planes with a tower readout geometry are inserted into each gap (Figure 8). The tower geometry was designed to allow convenient logical formation of Eperp and total hadronic energy triggers.

3.4 Trigger

3.4.1 First Level Trigger

The most important aspect of triggering in a photon experiment is to identify a probable hadronic event while suppressing the large number of pairs which are produced (primarily in the target and microstrips). The pairs have virtually no transverse momentum . They occupy a region the size of the beam until they pass through the first analysis magnet where they are spread vertically in a swath with the same horizontal width as the beam. The pairs are refocussed by the second analysis magnet (M2) into a spot roughly the size of the beam in the vicinity of the beam gamma monitor although there is some spread in spot size due to energy loss in the spectrometer. The trigger attempts to exploit the topological difference of the highly localized distribution of pairs and the relatively large spread of hadronic events. The counters TR1, TR2, OH and H x V formed the primary interaction trigger (Figure 9). TR1 and TR2 were scintillation counters placed downstream of the target and microstrips respectively and were used to define an interaction in the target. The OH and H x V's were arrays of counters used to reject electromagnetic interactions and to

identify hadronic events. The OH counters, located on the upstream face of the OE electromagnetic calorimeter, were used to detect wide angle charged particles. The H x V array was placed downstream of P4 with a 7.6 cm gap which allowed a majority of the pairs to pass through undetected.

The logic of the H x V hodoscope defined two triggers:

One or more hits = $(H \times V)_1$ (1-body)

Two or more hits = $(H \times V)_2$ (2-body)

These were combined with TR1•TR2 = T and OH to form the basic interaction trigger. A set of counters (AM, A0 and TM) were used to veto any charged particles in and around the beam. These were mostly beam halo muons and pair conversions from secondary photons.

The first level trigger was thus defined by:

$$\overline{(A0+AM+TM)}\bullet(T\bullet(H \times V)_2 + T\bullet(H \times V)_1\bullet OH)$$

3.4.2 Second Level Trigger

The second level trigger was composed of several trigger "sets". The main trigger set consisted of:

1) A RESH energy requirement which served to set a lower photon energy limit.
2) A PWC multiplicity requirement. This was used to further eliminate "pair" events.
3) A total hadronic energy requirement. An energy requirement of greater than 35 GeV suppressed the first level trigger rate by a factor of 100. The efficiency is shown in Figure 10.

Other trigger sets included muon triggers, and prescaled pair and minimum bias (first level) triggers for monitoring.

The hadronic fraction was approximately 50% for events written to tape which yielded roughly 1 fully reconstructed charm event for every 2400 reconstructed hardonic events.

3.4.3 Data Acquisition

Data from the detector was divided into 5 streams:

1) TDC's from MWPC's
2) Microstrips
3) OE ADC's
4) IE, HC, Cerenkov ADC's
5) Miscellaneous, including muon prop tubes, latches, etc.

Each stream was read into a 4 Mb LeCroy 1892 Fastbus buffer memory. The data for each memory was readout by a PDP 11/45 which combined the 5 streams into an "event" and wrote the data onto 9-track tape. Event monitoring was accomplished by a VAX 11/780. During a

typical 22 second spill we recorded 3000 events with a nominal size of two kbytes.

4.0 Event Reconstruction

The primary data reconstruction was performed on the Fermilab Advanced Computer Program (ACP) microprocessor system. Using a 60 node system events were processed at a rate of approximately 6-7 per second. Running on two systems the initial reconstruction of the 1200 9-track data tapes took less than three months.

The primary event reconstruction ("Pass1") consisted of proportional chamber and microstrip tracking and vertexing as well as particle identification using the Cerenkov system, calorimetry and muon detectors. Some cuts were made based on data quality. The resulting data was then reduced and subdivided in subsequent "skims" for further physics analysis.

4.1 Tracking

4.1.1 PWC tracking

Four categories of tracks were considered:

1) 5-chamber - Tracks which traverse the entire spectrometer.
2) 3-chamber (stubs) - Tracks in P0-P2. These are mainly low momentum particles swept out by the higher kick of M2.
3) Very low momentum tracks swept out by M1 (unlinked SSD tracks).
4) vee's and kinks from decays downstream of P0.

The main reconstruction routine was used to find 3 and 5-chamber tracks. Projections were formed using the hits in the U, V, Y (bend) views from PWC information alone. In the non-bend view X-projections were formed by using SSD track extensions as a "seed" to find all matching hits in the PWC's. Tracks were formed by matching all four projections. X-projections were then made from all unused PWC hits and combined with all unused U,V,Y-projections to form tracks. Final track selection was made on the number of hits and a χ^2 cut. The main algorithm was augmented by several additional routines designed to recover tracks in other categories. The tracking efficiency was greater than 98% for tracks with momentum greater than 5 GeV with reconstruction of spurious tracks occurring on the 0.5% level.

4.1.2 Microstrip Tracking

A simple analysis is first performed using charge interpolation in order to breakup clusters of hits from a number of closely spaced particles. The tracking then proceeds, using very loose cuts, by combining projections of at least three hits in each of the three separate views. A cut is made on the space tracks at a χ^2 per degree of freedom of 8. Space tracks which share views are arbitrated based on their χ^2. All the unused hits are used to search for wide angle tracks and for single segments of highly Coulomb

scattered tracks. The conservative approach of the algorithm often generates clusters of closely spaced tracks which are then reduced on the basis of the number of shared hits and their degrees of freedom. The operation is time consuming but is relatively free of bias. The reconstruction efficiency of the tracking algorithm was evaluated by a full Monte Carlo simulation of the microstrip system. The efficiency depends on the momentum as well as the number of degrees of freedom and was found to be 96% for simulated $D/\bar{D}$ production which included multiple scattering effects. The track reconstruction efficiency has a value of 90% for a 2.5 GeV track and reaches 99% at 10 GeV and above.

4.1.3 Linking

The microstrip and spectrometer tracks were linked as a means of improving the track momentum resolution and impact parameter resolution at the target. In addition, unlinked PWC tracks served as useful candidates for vee's and kinks and unlinked microstrip tracks were useful for reducing background in searching for charm decay. Links were made by comparing the microstrip and PWC track positions at the center of M1 and subjecting the potential links to a global least squares fit using all the hits.

4.2 Vertexing

The vertex reconstruction uses two primary techniques. The first method reconstructs all possible event verticies and has the least bias. The second method is a candidate driven algorithm which selects a particular decay channel and uses the candidate track parameters as a seed to find the primary vertex. Figure 11 illustrates the efficiency of vertexing in reducing combinatoric background.

4.3 Neutral Vees

There were several vee finding algorithms employed in the experiment because of the large number of distinct decay topologies. There were 4 separate decay regions considered in the vee analysis: Upstream of the microstrip detector (SSD vees), inside the microstrip detector (Mic vees), between the first chamber (P0) and the microstrip detector (M1 vees), and between P0 and P2 (reconstruction vees). Figure 12 shows K°_{s} signals in each of the 4 regions. Over a million K°_{s} were reconstructed with 25% utilizing SSD information.

4.4 Particle Identification

4.4.1 Cerenkov

A digital algorithm determined if each counter was off, on or confused for each track that passed through its fiducial volume and compared the pattern for consistency with being an electron, pion, kaon or proton. Typical analyses defined a K as K or K/P consistent up to 61 GeV. The range could be extended to 116 GeV by allowing a K to be K/π

consistent. The Cerenkov performance was determined by comparison with Monte Carlo and by looking at specific states in data with and without identification cuts such as K^o_S, Λ, ϕ and D^{*+}. The kaon identification efficiency was between 70 and 80% depending on decay mode within the momentum range of the system. The probability of misidentification of a pion as a kaon was about 4%. Figure 13 shows the effect of a Cerenkov requirement on the $D^{\pm}$ signal.

5.0 Current Status

The analysis of data from the 1988 run is well underway. Some preliminary results will be presented at this conference [3,4,5,6]. Another run is currently in progress with an improved spectrometer and should increase the data set by more than a factor of 5 over the previous run.

Acknowledgements

We wish to acknowledge the assistance of the staffs of Fermilab, INFN of Italy and the physics departments of the University of Colorado, University of Illinois, and University of Notre Dame. This research was supported in part by the National Science Foundation, the U.S. Department of Energy, the Italian Istituto Nazionale di Fisica Nucleare and Ministero della Universita'e della Ricerca Scientifica.

Footnotes

(a) Present address: IBM TJ Watson Laboratories, Yorktown Heights, NY 10598

(b) Present address: University of Oklahoma, Norman, OK 73019, USA

(c) Present address: University of North Carolina, Ashville, NC 28804, USA

(d) Present address: Fermilab, Batavia, IL 60510, USA

(e) Present address: Dipartmento di Elettronica, Universita' di Pavia, Pavia, Italy

(f) Present address: Universita di Pavia and INFN, I-27100 Pavia, Italy

(g) Present address: University of Alabama, University, AL 35486, USA

References

[1] Tagged Photon Beam design report, C. Halliwell et al., Nucl. Instr. and Methods, 102, 51 (1972)

[2] Wide Band Beam Design Report, Fermilab TM, no. 963

[3] "Photoproduction of D Mesons", submitted to this conference by D. Buchholz for the Fermilab E-687 collaboration.

[4] "D^+, D^0 Signals and Lifetimes in the E-687 Photoproduction Experiment at Fermilab", submitted to this conference by L. Moroni for the Fermilab E-687 collaboration.

[5] "Measurement of the J/Psi Elastic Photoproduction from 100 GeV to 400 GeV in Experiment E-687 at Fermilab", submitted to this conference by S.P. Ratti for the Fermilab E-687 collaboration.

[6] "Some Lifetimes and Branching Ratios for Charmed Hadrons Produced in the Fermilab Wide Band Photon Beam", submitted to this conference by W.D. Shephard for the Fermilab E-687 collaboration.

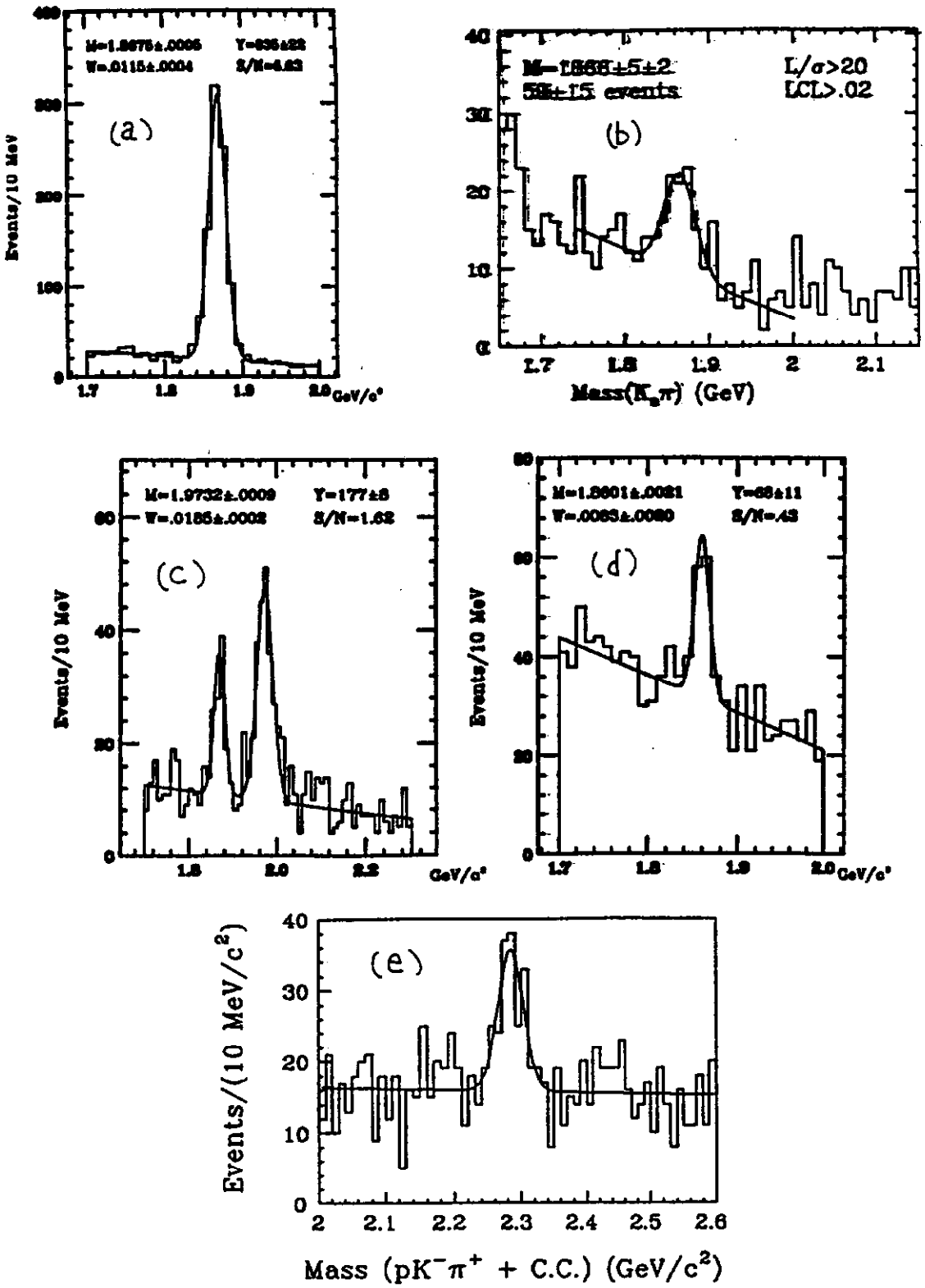

Figure 1: Some preliminary signals seen in E-687. (a) $D^{\pm} \to K^{-}\pi^{+}\pi^{+}$, (b) $D^{\pm} \to K^{\circ}_{S}\,\pi^{\pm}$, (c) $D^{+} \to \phi\pi^{+}$, $D^{+}_{S} \to \phi\pi^{+}$ (d) $D^{\circ} \to 4\pi$ (e) $\Lambda_{c} \to pK^{-}\,\pi^{+}$

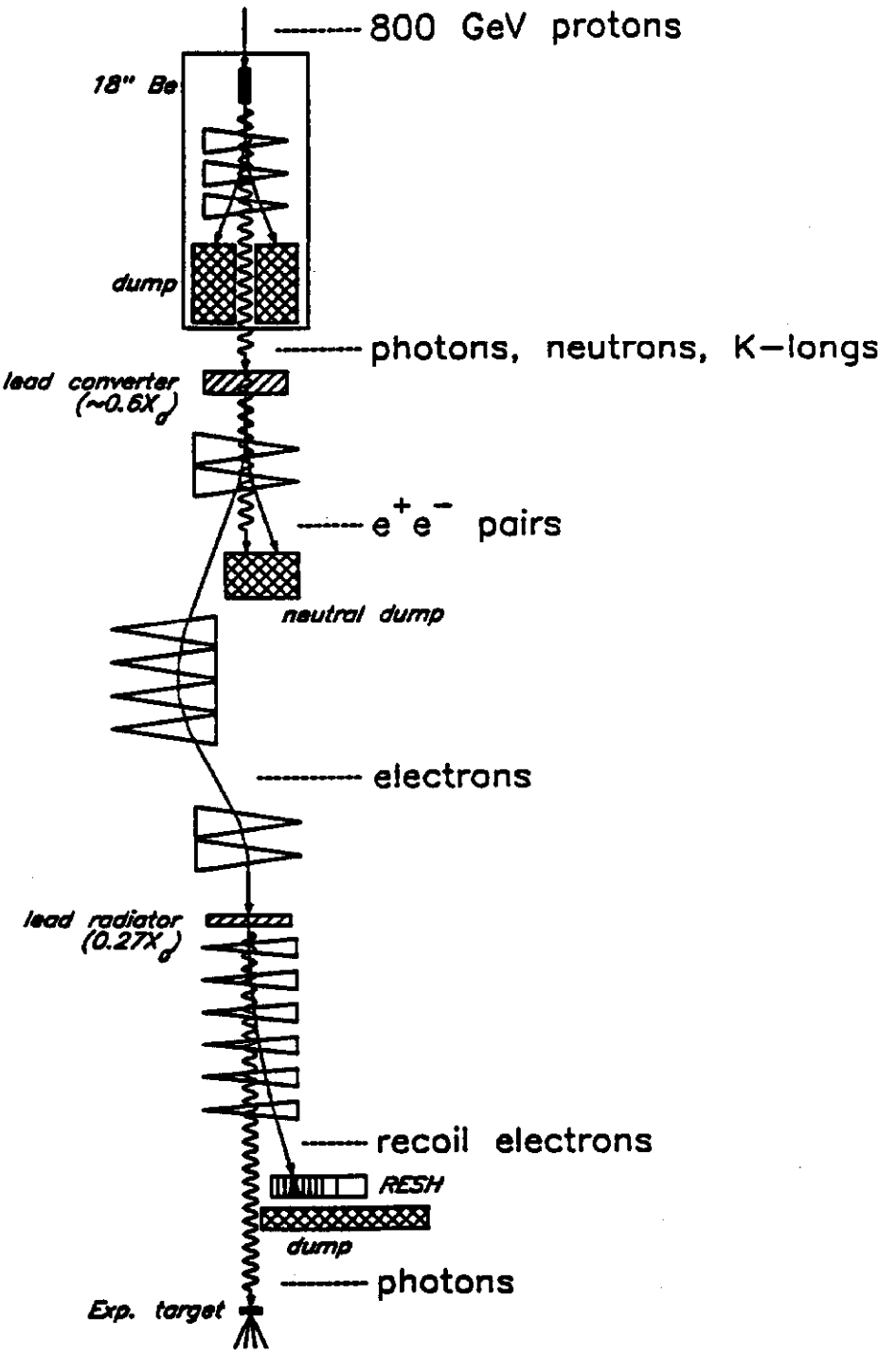

Figure 2: The Fermilab Wide Band Beamline.

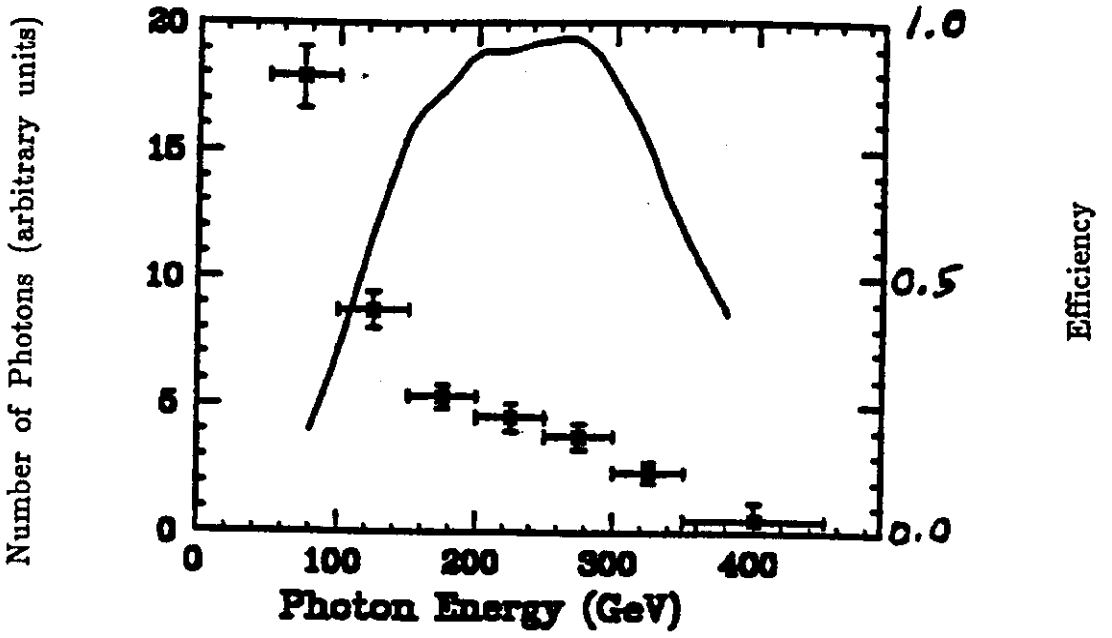

Figure 3: Photon energy spectrum (points, left scale). RESH acceptance (solid line, right scale).

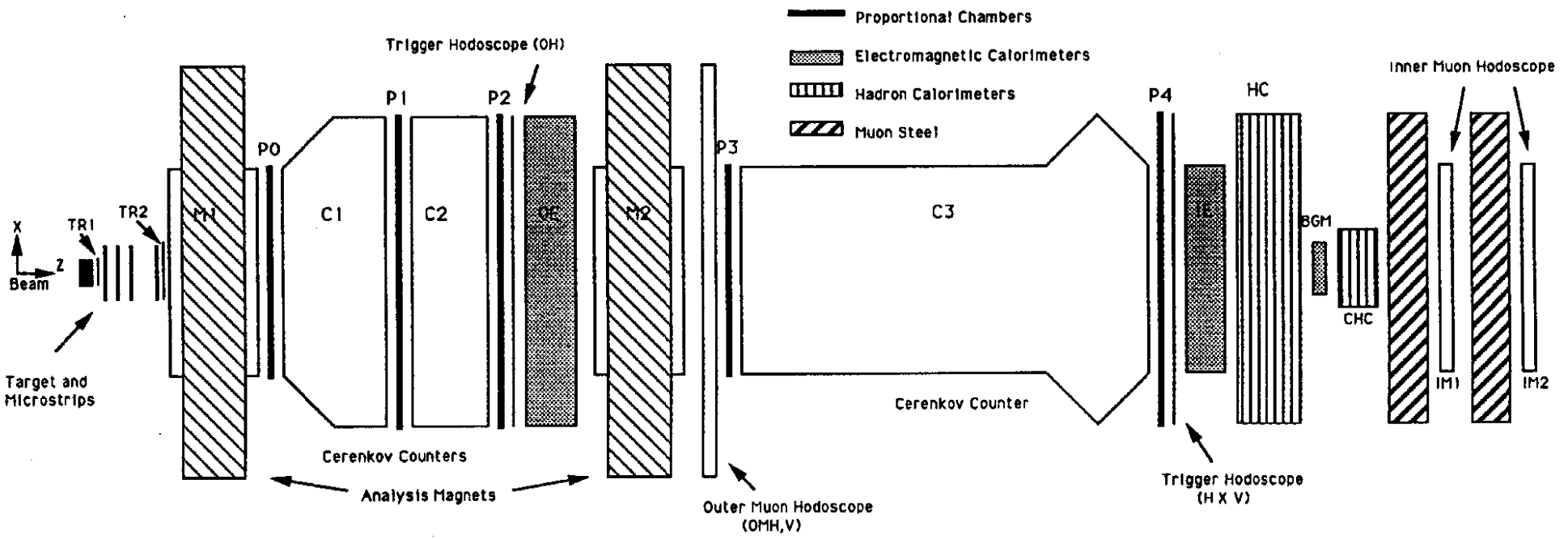

Figure 4: Plan view of the E-687 spectrometer. It is approximately 35 meters long and the target region occupies about 40 cm.

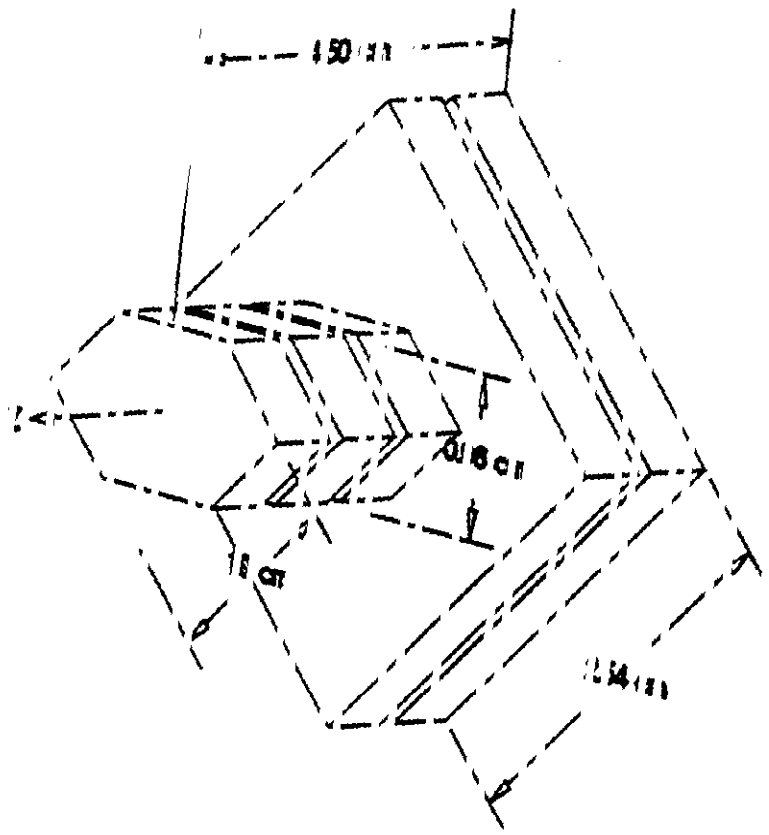

Figure 5: U-687 Beryllium Target.

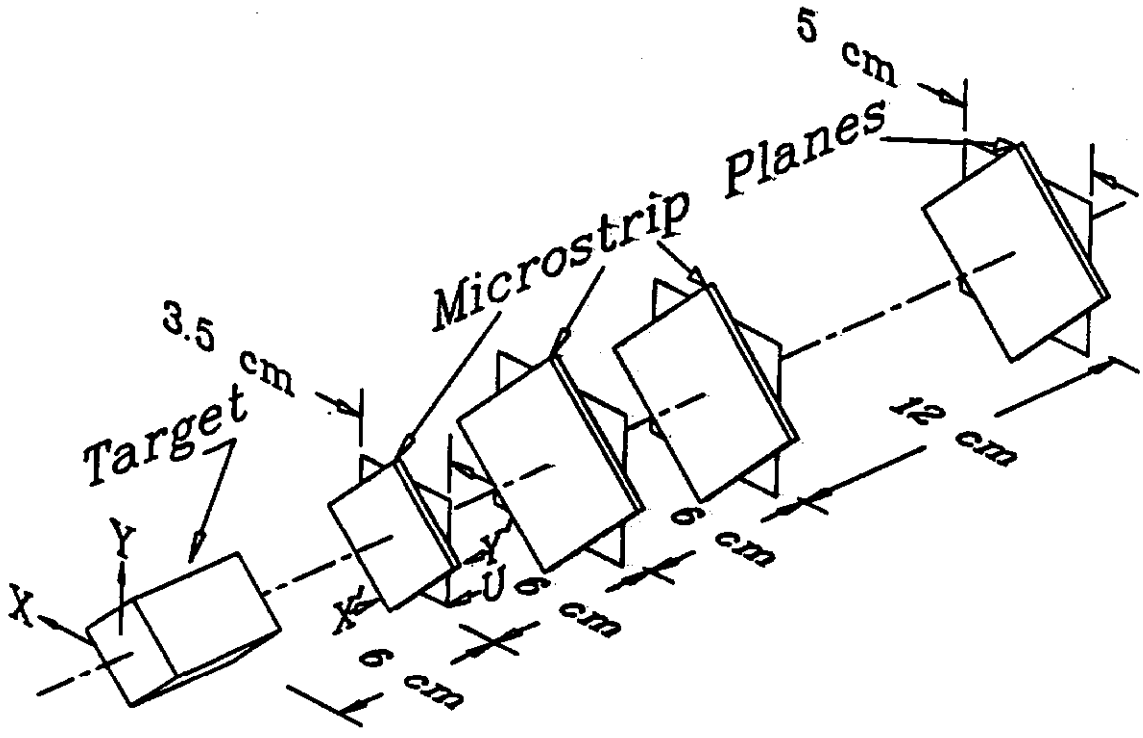

Figure 6: Silicon microstrip detector system.

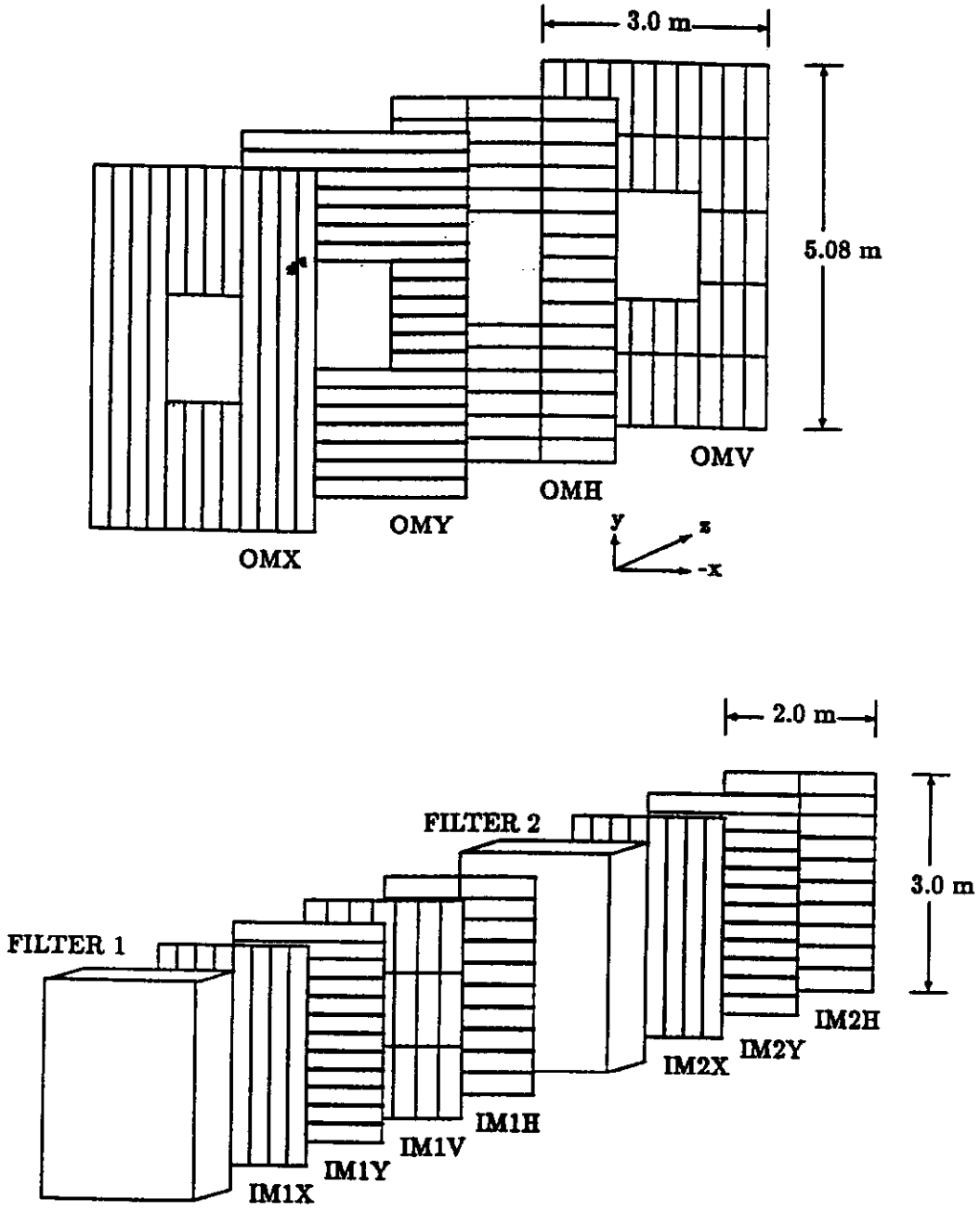

Figure 7: Muon detector system. Refer to Figure 3 for relative Z positions.

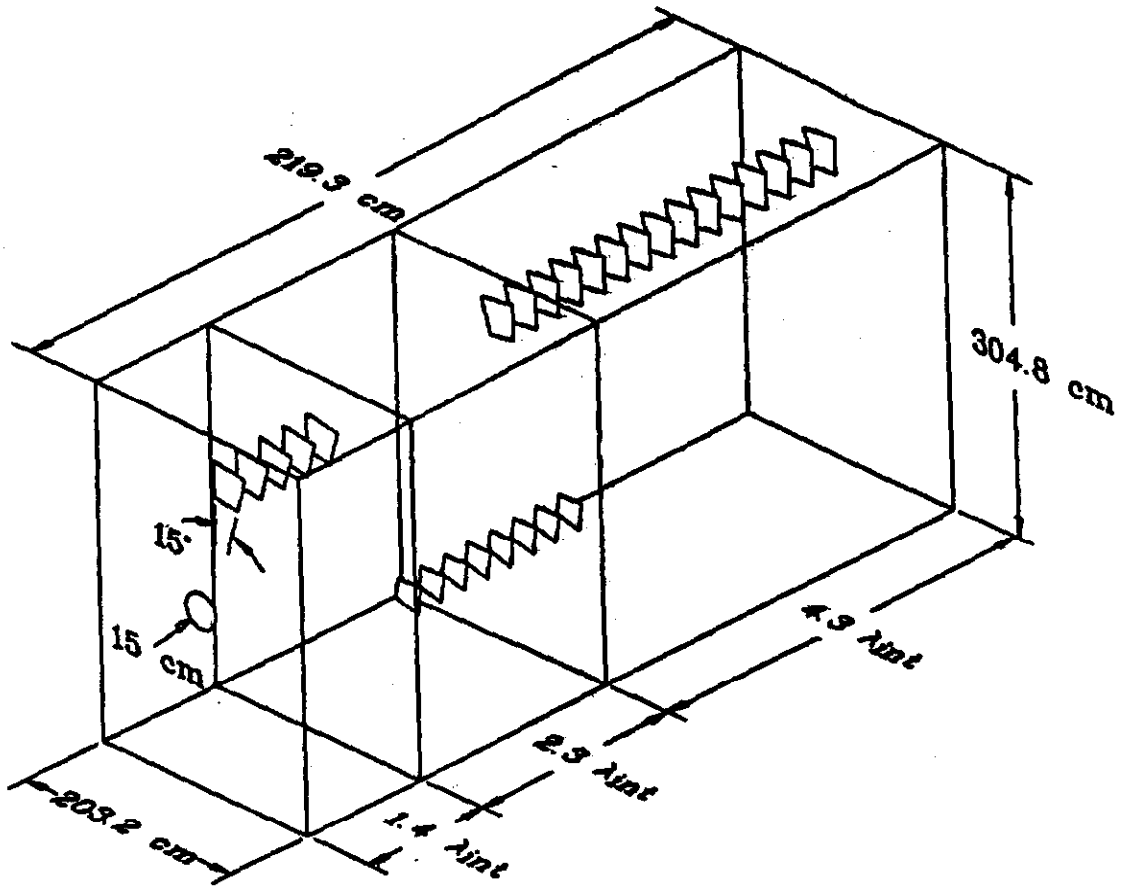

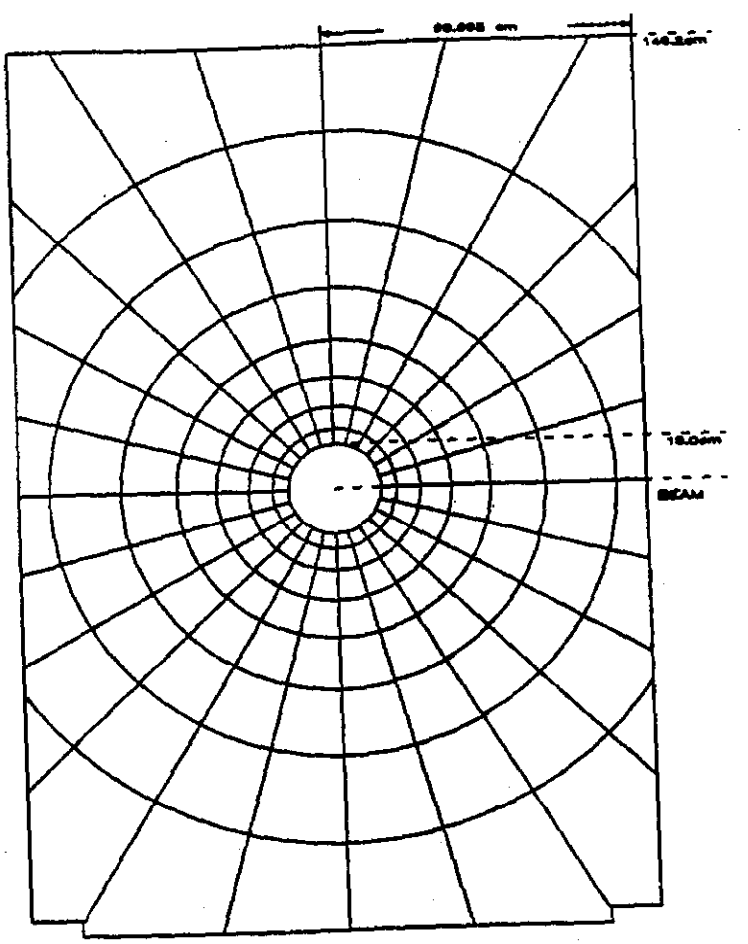

Figure 8: Hadron calorimeter and readout pad geometry.

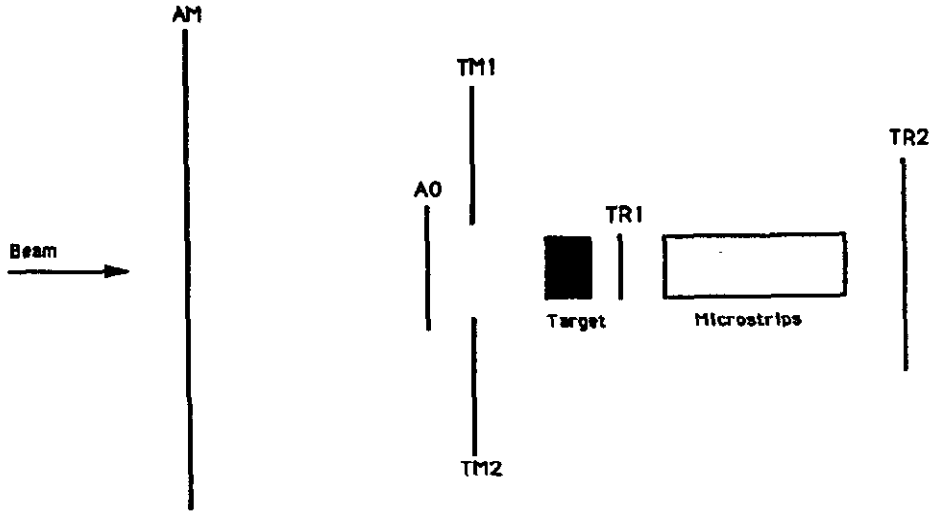

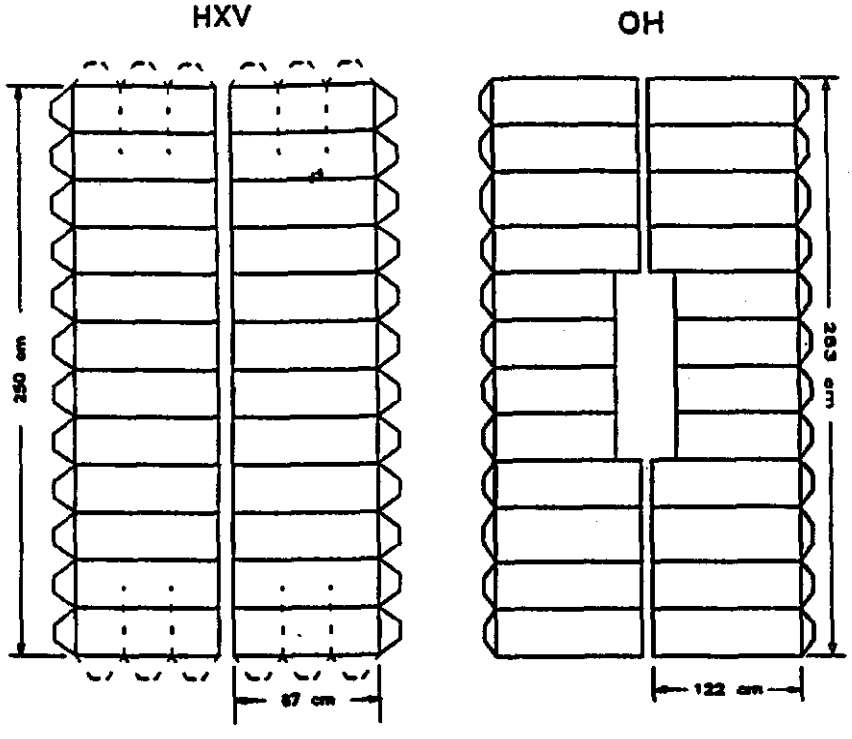

Figure 9: First level trigger counters. Refer to Figure 3 for relative Z positions.

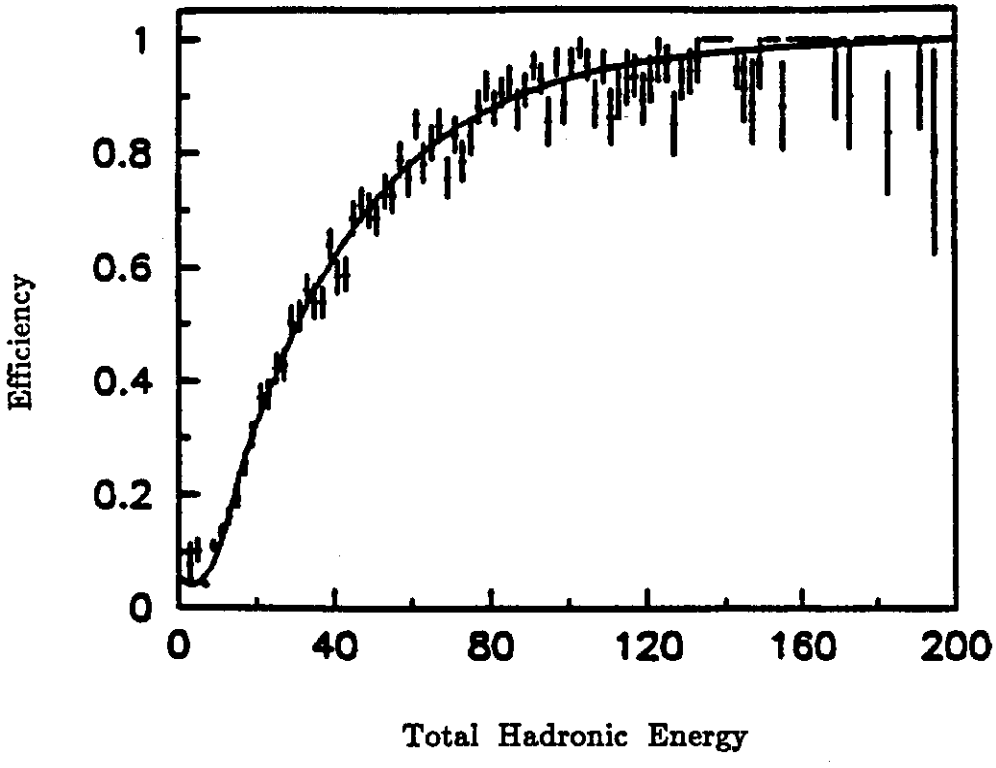

Figure 10: Hadron calorimeter efficiency.

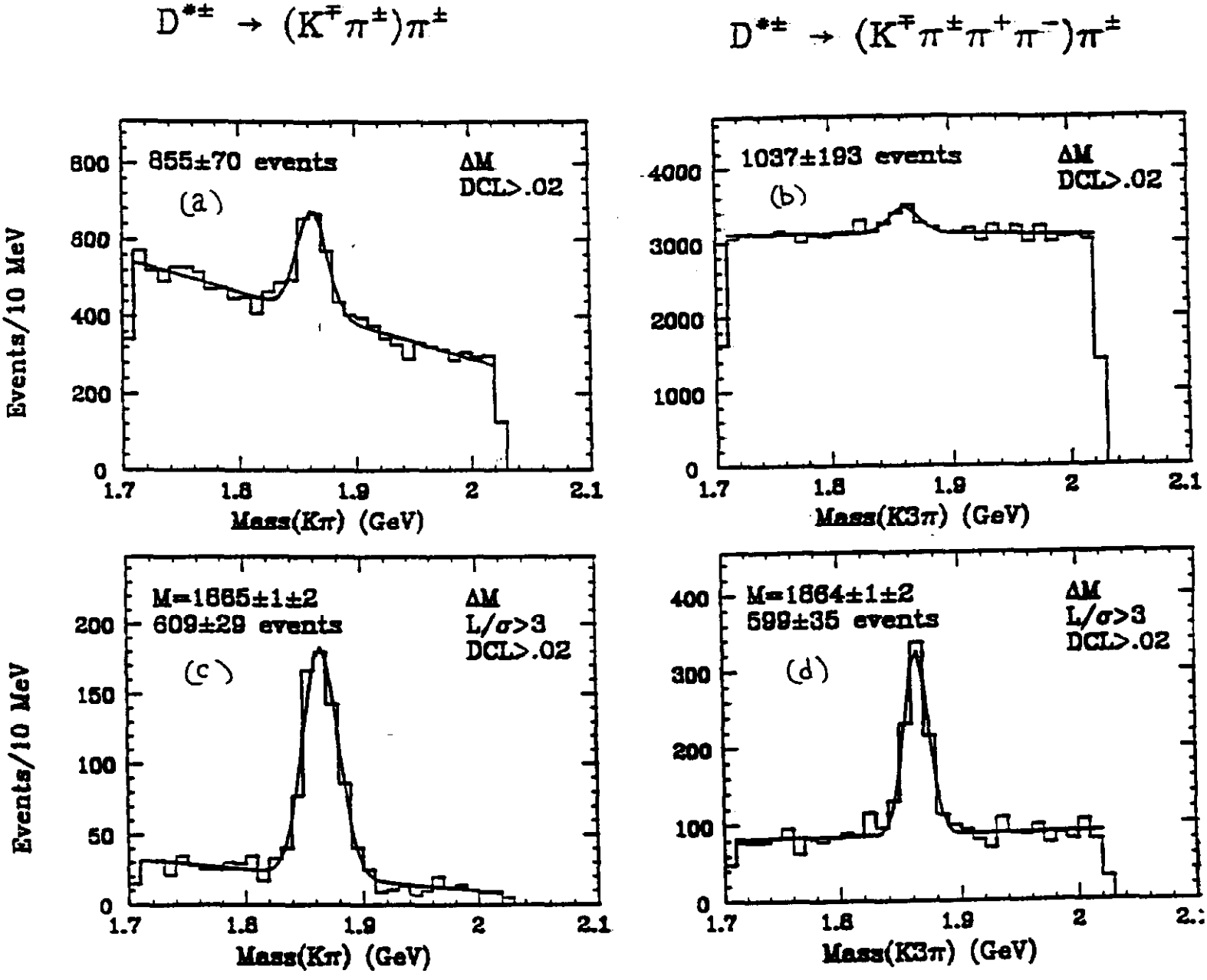

Figure 11: Effect of vertex separation cuts on

$$D^{*\pm} \to \left(K^{\mp}\pi^{\pm}\right)\pi^{\pm}, \quad D^{*\pm} \to \left(K^{\mp}\pi^{\pm}\pi^{+}\pi^{-}\right)\pi^{\pm}.$$

(a,b) Cerenkov, D^{*},D^{0} mass difference and secondary vertex requirements, (c,d) vertex separation cut imposed.

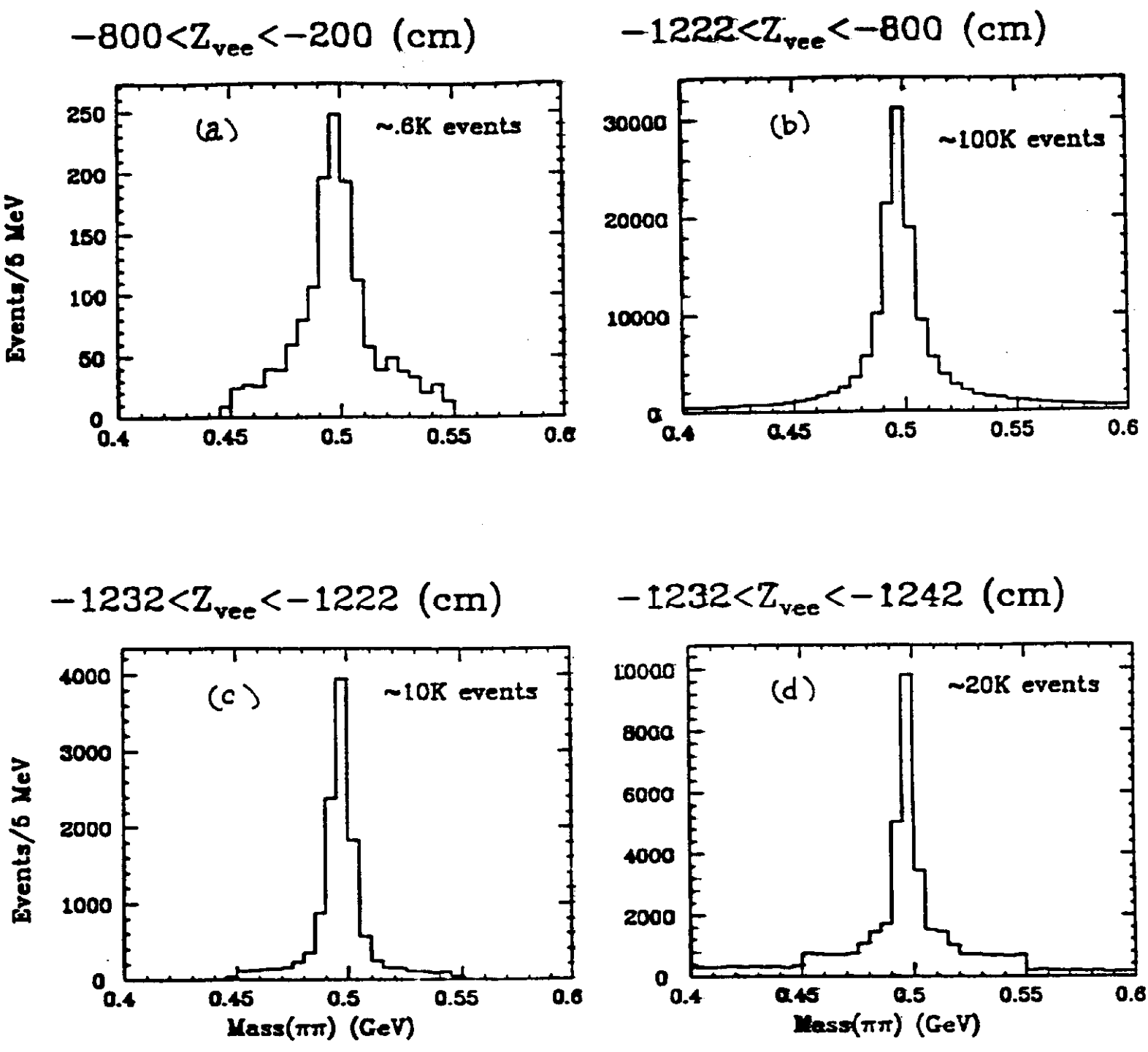

Figure 12: Examples of K°_{s} mass distributions over the 10m decay path. Center of M2 is defined as Z=0, and the target center is at -1242 cm. (a) between P0 and P2, (b) between P0 and the SSD's (c) inside the SSD's and (d) upstream of the SSD's.

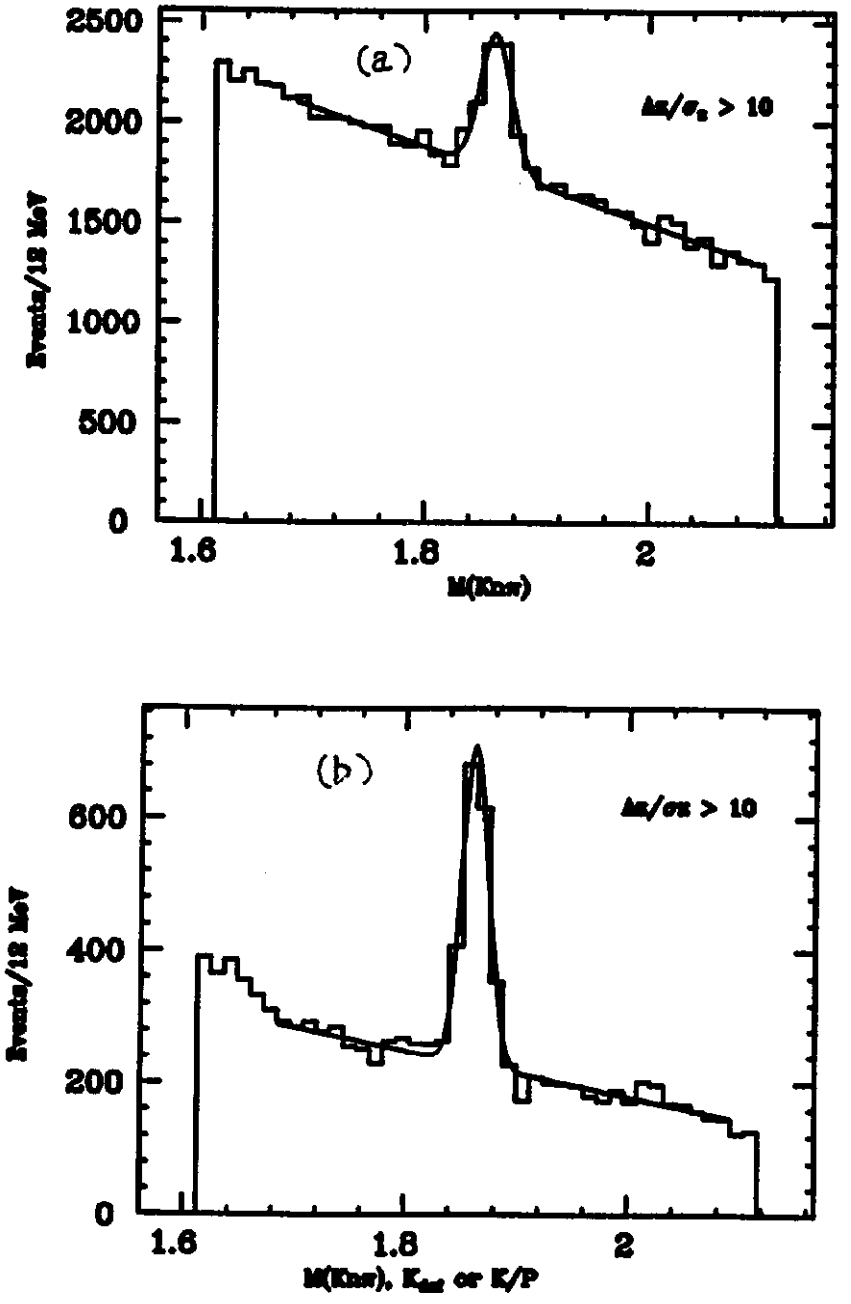

Figure 13: Effect of Cerenkov requirements on D° -> K(nπ). (a) no Cerenkov cut, (b) requirement of K definite or K/p ambiguous.